Conformational dynamics and intersubunit energy transfer in wild-type and mutant lipoamide dehydrogenase from *Azotobacter vinelandii*

A multidimensional time-resolved polarized fluorescence study

Philippe I. H. Bastiaens,* Arie van Hoek,‡ Jacques A. E. Benen,* Jean-Claude Brochon,§ and Antonie J. W. G. Visser*‖

Departments of *Biochemistry and ‡Molecular Physics, Agricultural University, 6700 ET Wageningen, The Netherlands; and §L.U.R.E., CNRS-CEA-MENJS, Centre Universitaire Paris-Sud Orsay F91405, France

ABSTRACT Time-resolved fluorescence and fluorescence anisotropy data surfaces of flavin adenine dinucleotide bound to lipoamide dehydrogenase from *Azotobacter vinelandii* in 80% glycerol have been obtained by variation of excitation energy and temperature between 203 and 303 K. The fluorescence kinetics of a deletion mutant lacking 14 COOH-terminal amino acids were compared with the wild-type enzyme to study a possible interaction of the COOH-terminal tail with the active site of the enzyme. The flavin adenine dinucleotide fluorescence in both proteins exhibits a bimodal lifetime distribution as recovered by the maximum entropy method of data analysis. The difference in standard enthalpy and entropy of associated conformational substates was retrieved from the fractional contributions of the two lifetime classes. Activation energies of thermal quenching were obtained that confirm that the isoalloxazines in the deletion mutant are solvent accessible in contrast to the wild-type enzyme. Red-edge spectroscopy in conjunction with variation of temperature provides the necessary experimental axes to interpret the fluorescence depolarization in terms of intersubunit energy transfer rather than reorientational dynamics of the flavins. The results can be explained by a compartmental model that describes the anisotropy decay of a binary, inhomogeneously broadened, homoenergy transfer system. By using this model in a global analysis of the fluorescence anisotropy decay surface, the distance between and relative orientation of the two isoalloxazine rings are elucidated. For the wild-type enzyme, this geometrical information is in agreement with crystallographic data of the *A. vinelandii* enzyme, whereas the mutual orientation of the subunits in the deletion mutant is slightly altered. In addition, the ambiguity in the direction of the emission transition moment in the isoalloxazine ring is solved. The anisotropy decay parameters also provide information on electronic and dipolar relaxational properties of the flavin active site. The local environment of the prosthetic groups in the deletion mutant of the *A. vinelandii* enzyme is highly inhomogeneous, and a transition from slow to rapid dipolar relaxation is observed over the measured temperature range. In the highly homogeneous active site of the wild-type enzyme, dipolar relaxation is slowed down beyond the time scale of fluorescence emission at any temperature studied. Our results are in favor of a COOH-terminal polypeptide interacting with the active site, thereby shielding the isoalloxazines from the solvent. This biological system forms a very appropriate tool to test the validity of photophysical models describing homoenergy transfer.

INTRODUCTION

Flavoproteins belong to a class of proteins with appropriate photophysical properties to study protein dynamics and structure by time-resolved fluorometric methods. The intrinsically fluorescent prosthetic group of most of these proteins is either flavin adenine dinucleotide (FAD)[1] or flavin mononucleotide, which both have the spectroscopically relevant isoalloxazine in common. The fluorescence properties of the isoalloxazinic ring vary largely among different flavoproteins, reflecting the variety in structure and dynamical properties of the active sites containing the flavin compounds (Visser et al., 1974, 1980, 1984; de Kok and Visser, 1987; Bastiaens et al., 1989).

The 100-kD flavoprotein lipoamide dehydrogenase of the class of disulfide-oxidoreductases has a dimeric quaternary structure containing one FAD per subunit. The protein catalyses the oxidized form of nicotinamide adenine dinucleotide-dependent oxidation of the covalently attached dihydrolipoyl groups of lipoate acyltransferase in different multienzyme complexes, such as the pyruvate dehydrogenase- and 2-oxoglutarate complex (Reed, 1974; Williams, 1976; de Kok and Visser, 1984; de Kok et al., 1988). This flavoprotein has several distinct advantages to study dynamics and structure by time-resolved fluorescence spectroscopy. First, it is a flavoprotein with an unusually high quantum yield of flavin fluorescence (240% of free FAD). Second, the gene encoding lipoamide dehydrogenase from *Azotobacter vinelandii* has been cloned and overexpressed in *Escherichia coli* (Westphal and de Kok, 1988), providing large quantities of protein and means to modify the physical properties of the active site near the fluorescent FAD. Third, the crystal structure of the *A. vinelandii* enzyme has been solved to 0.22 nm resolution that enables topological comparison with different spectroscopic methods (Mattevi et al., 1991).

Previously, fluorescence studies have been performed on lipoamide dehydrogenase from pig heart and from bacterial sources (Wahl et al., 1975; de Kok and Visser, 1987; Visser, 1989). The fluorescence decay was shown to be slightly heterogeneous and could be fitted to a triple exponential decay model. The fluorescence anisotropy decay was composed of two components. One correla-

‖ Address correspondence to Antonie J. W. G. Visser.

[1] *Abbreviations used in this paper:* CS, conformational substate; FAD, flavin adenine dinucleotide; FWHM, full width at half maximum; Lip(SH_2), reduced lipoamide; LipDH-AV, lipoamide dehydrogenase from *Azotobacter vinelandii;* LipDH-Δ14, deletion mutant of lipoamide dehydrogenase from *Azotobacter vinelandii;* MCS, multichannel scaling; MEM, maximum entropy method.

0006-3495/92/09/839/15 $2.00

tion time was assigned to protein rotation in the solvent, but the physical origin of the correlation time of ~12 ns with small amplitude was unclear and was tentatively assigned to restricted subunit motion.

In this study we have examined the time-resolved fluorescence of lipoamide dehydrogenase from *A. vinelandii* (LipDH-AV) and a deletion mutant of LipDH-AV, lacking 14 COOH-terminal amino acids (LipDH-Δ14) (Schulze et al., 1991). 10 COOH-terminal amino acids of LipDH-AV are not visible on the electron density map from which it was concluded that they are disordered (Mattevi et al., 1991). However, recently it was also proposed that a COOH-terminal polypeptide of 10 amino acids in lipoamide dehydrogenase from *Pseudomonas putida* is in interaction with the binding cleft of dehydrolipoamide (Mattevi, A., personal communication). This interaction possibly also occurs in LipDH-AV as is substantiated by the large influence of the solvent on the dielectric properties near the flavin in LipDH-Δ14, in contrast to the wild-type enzyme (Bastiaens et al., 1992*a*). This solvent effect causes an increased statistical spread in the electronic energy levels of ground and excited state (inhomogeneous broadening), reflecting the multiple solvent dipole configurations interacting with the chromophore (Rubinov and Tomin, 1970; Demchenko, 1987). A comparative time-resolved polarized fluorescence study of both wild-type and deletion mutant of lipoamide dehydrogenase will lead to insight in the dynamic structure surrounding the flavins and will assist in the verification of existing theories on spectral inhomogeneous broadening, dipolar relaxation, and energy transfer.

In the last decade, both time-correlated single-photon counting and multifrequency phase fluorometry became highly sophisticated, enabling data collection with a high signal to noise ratio and data density (Gratton et al., 1984; O'Connor and Phillips, 1984; Lakowicz et al., 1986; van Hoek et al., 1987). In conjunction with this development, considerable improvements in data analysis emerged over the classical treatment of fitting fluorescence decays by a sum of discrete exponentials. Two main approaches have appeared. The inverse Laplace transform of the fluorescence or fluorescence anisotropy decay is obtained by fitting the data to a distribution of parameters in the maximum entropy method (MEM) (Livesey and Brochon, 1987; Mérola et al., 1989; Gentin et al., 1990). The advantage of this method is that no a priori knowledge of the distribution model is needed. This type of analysis is well suited for complex fluorescence decay behavior encountered in biological macromolecules where multiple interchanging conformations give rise to semicontinuous sets of lifetime distributions. When a priori knowledge of the system is present, multiple fluorescence decays, as a function of different experimental independent variables (temperature, excitation wavelength), can be analyzed with global analytical procedures to a model encompassing multiple interrelated parameters. This computational method, which exploits the physical invariants of a model, allows for better model discrimination and parameter recovery than multiple single curve analysis (Beechem and Gratton, 1988; Beechem et al., 1991). In this study both methods of data analysis are applied to the fluorescence and fluorescence anisotropy decays of lipoamide dehydrogenase in highly viscous media.

The goal of this investigation is threefold: (*a*) to obtain insight in the kinetic and thermodynamic properties of conformational substates in lipoamide dehydrogenase, (*b*) to ascertain whether the short component in the anisotropy decay may originate either from intersubunit energy-transfer between the FAD prosthetic groups or from restricted flavin motion, and (*c*) to investigate the influence of dipolar relaxation and site selective excitation on energy transfer. To achieve this goal, we have measured time-resolved polarized fluorescence of the enzymes in 80% glycerol as function of temperature and excitation energy.

MATERIALS AND METHODS

Biochemical preparations

The plasmid-encoded LipDH-AV and deletion mutant LipDH-Δ14 expressed in *E. coli* TG2 were purified as described before (Westphal and de Kok, 1988). The enzyme preparations were stored at −70°C in 100 mM potassium phosphate buffer, pH 7.0, 0.5 mM ethylenediaminetetraacetate. The samples were defrosted at room temperature the morning before an experiment, and 300-ml aliquots were chromatographed on a column (1 × 6 cm, Biogel PGD-6; Bio-Rad Laboratories, Richmond, CA) equilibrated with 250 mM potassium phosphate buffer, pH 7.0, to eliminate unbound FAD. All buffers were made with nanopure water prepared on a water purification system (Millipore Continental Water Systems, Bedford, MA). The enzyme preparations were brought to 80% (vol/vol) glycerol by gently mixing 100 ml from the eluted sample with 400 ml of 100% glycerol (fluorescent grade, Merck, Darmstadt, Germany) until a homogeneous solution was obtained. Enzyme concentrations were determined with a molar extinction coefficient of $\epsilon_{457} = 11.3\ mM^{-1}\ cm^{-1}$ (Westphal and de Kok, 1988). Care was taken that all final preparations had a concentration of 10–15 mM.

FAD was purified on a Biogel P-2 (Bio-Rad). 100-ml aliquots of this preparation were mixed with 400 ml glycerol to a final concentration of 10 μM.

Instrumental

Decays of fluorescence and fluorescence anisotropy were measured using the time-correlated single photon counting technique (O'Connor and Phillips, 1984). For excitation with light of either 514.5 or 457.9 nm, a mode-locked cw argon-ion laser was used (model CR18, Coherent Inc., Palo Alto, CA). The rate of the light pulses was decreased from 76 MHz to 596 kHz by an electrooptic modulator set-up in a dual-pass configuration (van Hoek and Visser, 1981). Excitation pulses were ~100 ps full width at half maximum with energies in the picojoule region.

Sample volumes were 0.5 cm^3, and 1-cm lightpath cuvets, placed in a thermostatted holder, were used. This holder was placed in a sample housing also containing optics. Extreme care was taken to avoid artefacts from depolarizing effects. At the front of the sample housing a Glan-laser polarizer was mounted, optimizing the already vertical polarization of the input light beam. The fluorescence was collected at an

angle of 90° with respect to the direction of the exciting light beam. Between sample and photomultiplier (microchannel plate, model 1645U, Hamamatsu Corp., Bridgewater, NJ) a single fast lens (uncoated fused silica), a rotatable sheet polarizer, a filter compartment, and a single focusing lens (uncoated fused silica) were placed.

The polarizer sheet was in a dc motor-driven ball-bearing holder with mechanical stops allowing computer controlled rotation (0.2 s) to parallel and perpendicular polarized detection of emission. The sheet polarizer was a polaroid type HN38 for the green to red region. Filters used for wavelength selection of emission were a KV 550 cut off and a 557.9-nm interference filter with 10-nm bandpass (Schott, Mainz, Germany). The sample and photomultiplier housings were home built. Polarizers were aligned carefully, and when measuring reference samples of known anisotropy, it was found that no correction factor was necessary (g-factor = 1).

For sample temperatures down to 203 K, a liquid nitrogen flow setup was used with a temperature controller (model ITC4, Oxford Instruments Inc., Oxford, UK). At these low temperatures, experiments can easily be disturbed by the depolarizing effect of condensation of water from the surrounding air on the cuvet. Therefore, the sample housing was extended in height and filled with a steady stream of the relatively heavy argon gas onto the cuvet walls. The final temperature of the sample appeared to be in balance with different heat sources (cold nitrogen, room temperature argon gas, the heater of the controller, and heat radiation), and care was taken to control the true sample temperature. Furthermore, the cuvets were exchanged by one of us wearing surgical gloves. In this way, samples could be easily exchanged over a period of a few hours without dew and ice problems.

Detection electronics were standard time-correlated single photon counting modules (O'Connor and Phillips, 1984). A photon frequency of 30 kHz (5% of 596 kHz) was used (Vos et al., 1987) to prevent pile-up distortion. Also other instrumental sources for distortion of data were minimized (van Hoek and Visser, 1985) to below the noise level of normal photon statistics. Measurements consisted of a number of sequences of measuring 10 s parallel and 10 s perpendicular polarized emission until a content in the data sets of 3.5×10^6 counts for the reference compound and 5×10^6 counts for the sample was reached. The time-window consisted of 1,024 channels at 20 ps/channel. For deconvolution of the data, the reference convolution method was used (Vos et al., 1987). The reference compound was erythrosine B in methanol. One complete measurement consisted of measuring the polarized fluorescence decays of the reference compound, the sample, the background, and again the reference compound. Background fluorescence decay was sampled at one-fifth of the time of the sample acquisition time and was always below 2% of the sample intensity. Manipulation and fitting of the data were performed on a microVAX computer.

Emission spectra at different temperatures were recorded using this same setup by replacing the optical filters between the sample and the photomultiplier by a computer controlled monochromator (2 tandemized 0.25m monochromators, F/3.5 model 82.410, Jarrell-Ash Div., Fisher Scientific Co., Waltham, MA) and adapting lenses. The sheet type polarizer in the detection pathway was placed under magic angle with respect to the polarization of the excitation light. Furthermore, emission photons (via a constant fraction discriminator; model 1428A, Canberra Industries, Meriden, CT) were not used now to trigger the start-stop sequence of the time to amplitude converter (model 457, Ortec, Oak Ridge, TN), but photon pulses via the constant fraction discriminator were directly fed to the multichannel scaling input of the multichannel analyzer [model ND66 equipped with both a ND582 analog to digital converter and a ZDT-MCS zero dead time multichannel scaling (MCS) unit, Nuclear Data Inc., Schaumburg, IL]. The channel stepping of the MCS was synchronized by the controller of stepper motor of the monochromator. The bandwidth of the monochromator was 6 nm for the spectra with 457.9 nm excitation and 1.5 nm for the spectra with 514.5 nm excitation. The emission spectra were converted from technical into molecular spectra using a computer program containing the transmission characteristics of the monochromator and the photomultiplier.

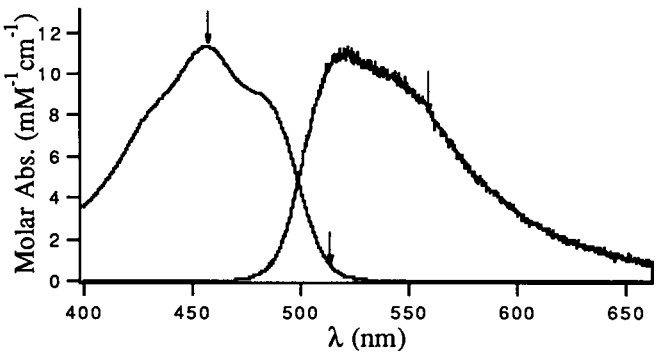

FIGURE 1 Absorption and emission spectra of LipDH-AV at 293 K in 80% glycerol, 50 mM KPi, pH 7.0. The arrows on the absorption spectrum indicate main band (457.9 nm) and red-edge (514.5 nm) excitation. The arrow on the emission spectrum is pointed at the maximal transmission of the interference filter used in the detection path. The emission spectrum was normalized to the maximum absorbance of LipDH-AV.

Temperature-dependent excitation spectra were recorded on a DMX-1000 (SLM Aminco, Urbana, IL). Spectra were recorded in the ratio mode to correct for the spectral output of excitation monochromator and lamp combination. The temperature in the sample holder was controlled by the same setup as used in the acquisition of the emission spectra described above. Both the excitation and emission bandwidths were set at 4 nm, and the emission detection wavelength was fixed at 580 nm. Overlap integrals between excitation and emission spectra were determined on a Macintosh SE/30 microcomputer using the program IGOR (wavemetrics).

Generation of fluorescence data surface

In Fig. 1 the normalized absorption and fluorescence spectra of LipDH-AV in 80% glycerol, 50 mM K_2HPO_4, pH 7.0, at 293 K are shown. The data surface was generated by collecting the parallel and perpendicular polarized component of the time-resolved fluorescence on separate excitations (457.9 and 514.5 nm) at 203, 223, 243, 263, 283, 293, and 303 K. Both polarized decays were collected in the 1,024 channels of a multichannel analyzer, temporarily stored in a PC, and transferred to the microVAX.

Data analysis

The data were analyzed with the commercially available second generation global analysis package (Globals Unlimited, Urbana, IL) and with the maximum entropy method (FAME, Maximum Entropy Data Consultants Ltd., Cambridge, UK). The principles of both analysis methods will be briefly outlined in relation to the protein system under investigation. The parallel $I_{\parallel}(t)$ and perpendicular $I_{\perp}(t)$ fluorescence intensity components were acquired after excitation with vertically polarized light. With the MEM, the image ($\alpha(\tau)$) of the total fluorescence intensity $i(t)$ after δ-pulse excitation is given by the Laplace transform (Livesey and Brochon, 1987):

$$i(t) = i_{\parallel}(t) + 2i_{\perp}(t) = \int_0^{\infty} \alpha(\tau) e^{-t/\tau}\, d\tau \qquad (1)$$

The image $\alpha(\tau)$ is recovered by maximizing the Skilling-Jaynes entropy function S_{SJ} (Livesey and Brochon, 1987):

$$S_{SJ} = \int_0^\infty \alpha(\tau) - m(\tau) - \alpha(\tau) \log \frac{\alpha(\tau)}{m(\tau)} d\tau \qquad (2)$$

and minimizing the χ^2 (data) fitting criterium:

$$\chi^2 = \frac{1}{M} \sum_{k=1}^{M} \left(\frac{I_k^{calc} - I_k^{obs}}{\sigma_k} \right)^2 \qquad (3)$$

where $m(\tau)$ is the starting model of the distribution chosen to be flat in log (τ) space because this introduces the least correlations between the parameters $\alpha(\tau)$ (Livesey and Brochon, 1987). The superscripts calc and obs on I denote the observed and calculated intensity in channel k of the multichannel analyzer, M is the total amount of channels used in the analysis of the fluorescence decay (typically 1,024 channels), and σ_k^2 is the variance in channel k. For an optimal fit of the data, χ^2 should approach unity. In the analysis of the total fluorescence decay of protein-bound FAD, 150 equally spaced values on a log (τ) scale between 0.01 and 20 ns were used. The starting model $m(\tau)$ was chosen to be flat in log (τ) space since no a priori knowledge about the system was present.

One is able to recover from fluorescence anisotropy experiments the complete three-dimensional image that is given by $\gamma(\tau, \phi, r_0)$, representing the number of fluorophores with lifetime τ, rotational correlation time ϕ, and initial anisotropy r_0 (Livesey and Brochon, 1987). If one assumes a priori that there is no correlation between τ and ϕ (nonassociative modeling), then the images $\alpha(\tau)$ and $\beta(\phi)$ are independent as shown for the parallel and perpendicular fluorescence intensity components:

$$i_{\parallel}(t) = \frac{1}{3} \int_0^\infty \alpha(\tau) e^{-t/\tau} d\tau \int_0^\infty (1 + 2\beta(\phi)) e^{-t/\phi} d\phi \qquad (4)$$

$$i_{\perp}(t) = \frac{1}{3} \int_0^\infty \alpha(\tau) e^{-t/\tau} d\tau \int_0^\infty (1 - \beta(\phi)) e^{-t/\phi} d\phi. \qquad (5)$$

The integrated amplitude $\beta(\phi)$ corresponds to the initial anisotropy r_0. In the (one-dimensional) anisotropy analysis, one obtains a spectrum of amplitudes β against correlation times ϕ. Similar considerations regarding the starting model in the recovery of $\alpha(\tau)$ apply to the recovery of $\beta(\phi)$, i.e., if one has no a priori knowledge of the distribution, then one should start with a flat spectrum in log (ϕ) space.

The final image $\alpha(\tau)$ of the fluorescence decay was introduced as a fixed image in the analysis of the anisotropy decay. As a starting model, 100 equally spaced values on a log (ϕ) scale (from 0.1 to 100 ns) were used in the analysis, and a limiting anisotropy was encoded since protein rotation is inhibited in 80% glycerol.

The following approach was used in the global analysis of the fluorescence and fluorescence anisotropy decay surfaces. The total fluorescence intensity curves were constructed from the parallel and perpendicular decay files (Eq. 1). Background fluorescence was subtracted from the data, and weighting factors were calculated as described by Vos et al. (1987). Multiple experiments were simultaneously analyzed using the model and parameter link schemes given in Results. The obtained fluorescence decay parameters were fixed in the analysis of the fluorescence anisotropy. Parallel and perpendicular decay files were subsequently constructed from the raw data with appropriate correction for background fluorescence and weighting. The fluorescence anisotropy surface was fitted to models described in the results section by a global approach where all parameters of the individual parallel and perpendicular polarized components were completely linked and simultaneously analyzed. In all cases, nonassociative modeling was used in the analysis of the fluorescence anisotropy decay. In the temperature- and excitation wavelength-dependent experiments, the linking schemes of fluorescence anisotropy parameters are given in Results. All fits were subjected to rigorous error analysis based on an exhaustive search along each parameter axis, allowing all other parameters to vary so as to find a minimum χ^2. This method takes into account all higher order correlation that may exist between the recovered parameters. From this analysis, the identifiability of a model and the standard error of the parameters can be determined (Beechem and Gratton, 1988).

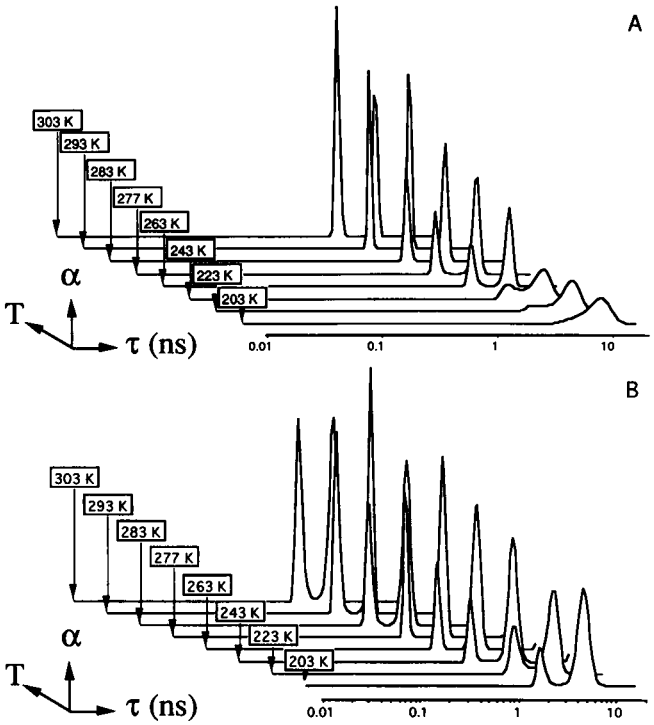

FIGURE 2 Temperature dependence of fluorescence decay of lipoamide dehydrogenase on 457.9 nm excitation in 80% glycerol, 50 mM KPi, pH 7.0. (*A*) Inverse Laplace transforms of fluorescence decays of LipDH-AV. (*B*) Inverse Laplace transforms of fluorescence decays of LipDH-Δ14.

RESULTS

Total fluorescence decay

The inverse Laplace transforms of the fluorescence decays of LipDH-AV and LipDH-Δ14 in 80% glycerol on 457.9-nm excitation (main-band) are represented as function of temperature in three-dimensional plots in Fig. 2. The residuals of the fits were randomly distributed around zero, indicating that the parameters of the lifetime spectra were optimized (data not shown). For both proteins a bimodal distribution in lifetime space was found with a tendency to collapse into a single broad distribution on lowering the temperature. The two lifetime classes of the protein-bound flavin cannot correspond to an equilibrium between "stacked" and "extended" FAD conformations (Spencer and Weber, 1972; Visser, 1984) since they are bound in an extended conformation (Mattevi et al., 1991). The possibility that the flavins have different lifetimes in each subunit of the protein can also be disregarded since a constant ratio of the integrated amplitudes would be expected at all temperatures. The two peaks in the lifetime spectrum can

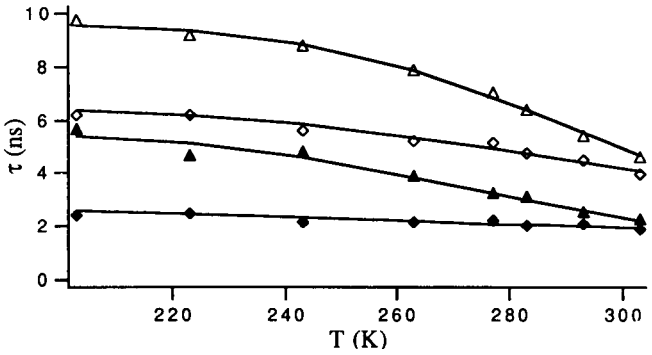

FIGURE 3 Temperature dependence of barycenters of the lifetime distributions. (▲) LipDH-AV, (♦) LipDH-Δ14, (△, ◇) Longest lifetime class, (▲, ♦) Shortest lifetime class, (——) Best fit of data to Eq. 8.

then be assigned to conformational substates of the protein. The fractional contributions of the peaks are proportional to the relative populations of these substates when the exchange between protein conformations (k_{exc}) is much slower than the depopulation of the excited state (k_f) (Alcala et al., 1987). Examination of the barycenters of the peaks (Mérola et al., 1989) as function of temperature (Fig. 3) shows that these do not converge on increase of temperature. Slow exchange between substates ($k_{exc} \ll k_f$) thus takes place in this temperature range.

From the ratio of the normalized fractional contribution of the peaks (α_1/α_2), the equilibrium constant (K) of conformational exchange is obtained. The standard enthalpy difference between states (ΔH^0) can then be calculated from the van 't Hoff equation:

$$\Delta H^0 = -R \frac{d \ln (\alpha_1/\alpha_2)}{d(1/T)}, \qquad (6)$$

where T is the temperature in Kelvin and R the gas constant (8.31 JK^{-1} mol^{-1}). The van 't Hoff plots of the equilibrium constants of protein-bound FAD are presented in Fig. 4. The plot of LipDH-Δ14 deviates from linearity below 263 K. At these temperatures, the conformational states in LipDH-Δ14 are not at equilibrium.

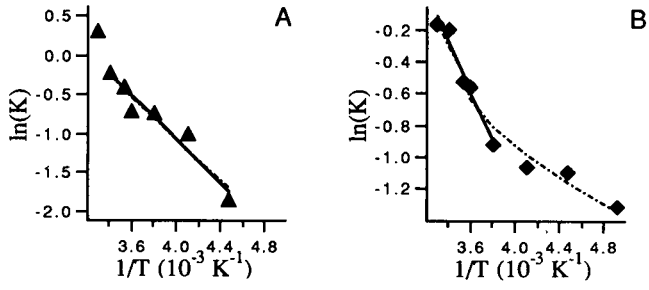

FIGURE 4 van 't Hoff plot of equilibrium constants of conformational transition. (*A*) Data for LipDH-AV. (*B*) Data for LipDH-Δ14. (——) Linear fit to experimental data.

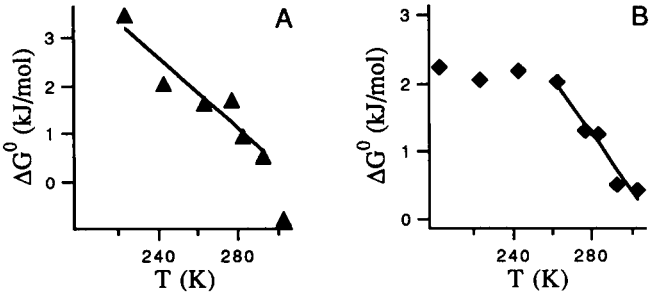

FIGURE 5 Free energy of conformational transition as function of temperature. (*A*) Data for LipDH-AV. (*B*) Data for LipDH-Δ14. (——) Linear fit to experimental data.

The activation barrier between states is apparently smaller in LipDH-AV since the van 't Hoff plot is linear over the whole temperature range (equilibrium attained). To determine ΔH^0, the linear part of the plot was used (203–303 K for LipDH-AV and 243–303 K for LipDH-Δ14). From the slope we found a ΔH^0 of 13.2 ± 1.5 kJ/mol for LipDH-Δ14 and 11.4 ± 1.5 kJ/mol for LipDH-AV. The standard entropy difference (ΔS^0) between states is obtained from the temperature dependence of the free energy (ΔG^0):

$$\frac{d\Delta G^0}{dT} = -\Delta S^0. \qquad (7)$$

ΔG^0 for both proteins is plotted as function of temperature in Fig. 5. From the slope of the plots, we obtained a ΔS^0 of 36 ± 6 JK^{-1} mol^{-1} for LipDH-AV (fit region: 223–293 K) and 42 ± 6 JK^{-1} mol^{-1} for LipDH-Δ14 (fit region: 263–303 K). Entropy increase is thus the "driving force" for the population of the conformational state associated with the smallest average lifetime.

From the plot (Fig. 3) of the barycenters as function of temperature, it can be seen that the flavins are located in different environments in both proteins. The fluorescence rate constants were not linear on Arrhenius coordinates (data not shown) and they approach to a constant value at low temperature. The deactivation of the excitation energy of the intrinsic fluorophores by adjacent residues is then governed by both thermally activated and temperature-independent radiative constants (Galley and Edelman, 1962):

$$\frac{1}{\tau_i(T)} = k_0^i + k_1^i \exp\left(\frac{-E_f^i}{RT}\right), \qquad (8)$$

where $\tau_i(T)$ is the lifetime of the flavin in conformation i at temperature T in ns, k_0^i is the temperature-independent rate constant in ns^{-1}, k_1^i is the frequency factor in ns^{-1}, E_f^i is the effective activation energy of thermal deactivation in J/mol. The barycenters were fitted to Eq. 8 with T as the independent variable (Fig. 3). In addition, a global analysis of the fluorescence decay surface

TABLE 1 **Fluorescence decay parameters**

	k_0^1	k_1^1	E_f^1	k_0^2	k_1^2	E_f^2
	GHz	*THz*	*kJ/mol*	*GHz*	*THz*	*kJ/mol*
LipDH-AV	0.18*	0.82*	20*	0.10*	3.2*	26*
	0.22‡	1.1‡	20‡	0.10‡	2.9‡	25‡
	(0.13–0.26)	(0.02–7)	(13–23)	(0.087–0.11)	(2–20)	(23–33)
LipDH-Δ14	0.35*	0.004*	7.5*	0.15*	0.063*	17*
	0.30‡	0.017‡	11‡	0.14‡	0.065‡	16‡
	(0.27–0.33)	(0.016–0.2)	(6.6–24)	(0.13–0.14)	(0.050–0.35)	(16–22)

* Values obtained by fitting the barycenters of the fluorescence lifetime distributions as function of temperature to Eq. 8.
‡ Values obtained from a simultaneous (global) analysis of eight decay curves. The numbers in parentheses are the errors obtained from a rigorous error analysis with 67% confidence.

assuming two noninteracting compartments was performed where eight fluorescence decays (203–303 K) were analyzed simultaneously with the k_0^i, k_1^i, and E_f^i ($i = 1, 2$) linked over all experiments. We obtained an optimized fit with global χ^2 of 1.08 and 1.09 for LipDH-AV and LipDH-Δ14, respectively. Both residual surfaces were randomized around zero, indicating a correct implementation of the model to the system (data not shown). Both types of analysis gave comparable results with the advantage of the global analysis that the error in the parameters can be estimated (Table 1). The two activation energies of thermal quenching in each individual conformation of both proteins are significantly different. The activation energy associated with the shortest lifetime class is smaller than the one associated with the longest lifetime class, indicating a more rigid local protein matrix surrounding the isoalloxazines in the conformation associated with the longer fluorescence lifetime. The difference in local amino acid residue dynamics in both states could account for the positive entropy difference as found from equilibrium thermodynamic considerations.

In the partially exposed isoalloxazine in LipDH-Δ14, interaction of the flavin with the solvent causes effective internal conversion to the ground state. This leads to an elevated temperature-independent rate constant, a smaller frequency factor, and smaller activation energy of thermal quenching as compared with the shielded flavin in the wild-type protein (Table 1).

The advantage of MEM in the analysis of the fluorescence data is that additional information can be extracted that is not a priori encoded in the analysis. An example is the full width at half maximum (FWHM) of the lifetime distributions that showed a trend with temperature (Fig. 6). In all of the experiments, the total number of counted photons was approximately equal. In that case one can reasonably assign a physical meaning to the relative widths of the distributions as recovered by MEM, since the signal to noise ratio should be comparable in every experiment. The FWHM of a lifetime class at temperature T is related to two factors: the number of conformational substates and the relative rate of interconversion between states. At 203 K the interconversion is assumed to be slow on a fluorescence time scale, and therefore the width is mainly determined by the number of conformational substates. This number can be ranked by the magnitude of the FWHM at the lowest temperature. By examining Fig. 6, *A* and *B*, it is clear that the population of conformational substates is largest in the wild-type enzyme. A decrease in the FWHM with temperature can be interpreted as an increase in the rate of exchange between subconformations. The half widths of

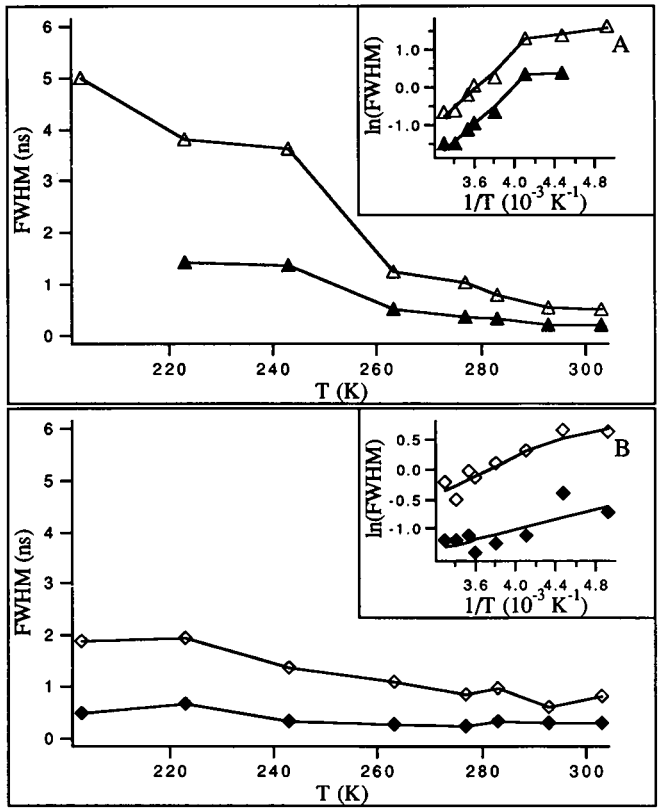

FIGURE 6 Full width at half maximum (FWHM) of lifetime distributions as function of temperature. (△, ◇) Longest lifetime class, (▲, ◆) Shortest lifetime class. (*A*) LipDH-AV. (*B*) LipDH-Δ14. (*Insets*) FWHM on Arrhenius coordinates.

the two lifetime distributions of LipDH-AV on Arrhenius coordinates show a clear breakpoint at 243 K (Fig. 6 *A*, inset). A similar transition at the same temperature is observed in the barycenters of the two lifetime distributions of LipDH-AV (Fig. 3). The empirical activation energy determined from the slope of the Arrhenius plot of the FWHM between 243 and 303 K is 20 ± 2 kJ/mol for both distributions. This energy is comparable with the activation energy of thermal quenching (Table 1). For LipDH-Δ14 the breakpoint at 243 K was less apparent but also present in the Arrhenius plot of the FWHM of the longer lifetime component (Fig. 6 *B*, inset). The activation energies were 4 ± 1 kJ/mol for the shorter lifetime component and 7 ± 2 kJ/mol for the longer lifetime component. These activation energies are lower than those of thermal quenching (Table 1) but demonstrate the smaller temperature dependence of the lifetime distributions of FAD bound to LipDH-Δ14. Quenching of flavin fluorescence is caused by collisional interaction with local amino acid residues that can be interpreted as a transition from one conformational coordinate to another. It can then be conceived that the transition between conformational substates, as reflected in the decrease of the FWHM, is the origin of the thermal quenching.

Fluorescence anisotropy decay

To ascertain whether another process than protein tumbling alone causes depolarization of fluorescence in lipoamide dehydrogenase and to obtain a qualitative insight in the physical origin of this depolarizing mechanism, we will focus on a few two-dimensional slices of the experimental anisotropy decay data surfaces of LipDH-AV and LipDH-Δ14. In Fig. 7 the fluorescence anisotropy decays of LipDH-AV in 80% glycerol at 203.15 (*A*) and 293 K (*B*) excited at 457.9 nm are depicted together with the anisotropy decays of free FAD under the same conditions. The fluorescence of the relatively small molecule FAD (596 D) does not depolarize at 203.15 K in the experimental time window, whereas the fluorescence of FAD bound to the large macromolecule LipDH-AV (100 kD) exhibits a clear depolarization. This shows that because protein tumbling is effectively abolished under such conditions, another process is causing depolarization of the fluorescence in LipDH-AV. At 293.15 K, the fluorescence of free FAD depolarizes because of Brownian molecular rotation, whereas in a first approximation the anisotropy decay of LipDH-AV can be superimposed to the one at 203 K. This lack of temperature variance is the first qualitative indication that the mechanism of depolarization is not due to restricted rotation but to intersubunit energy transfer between the flavins. The same phenomena were observed for LipDH-Δ14 (data not shown).

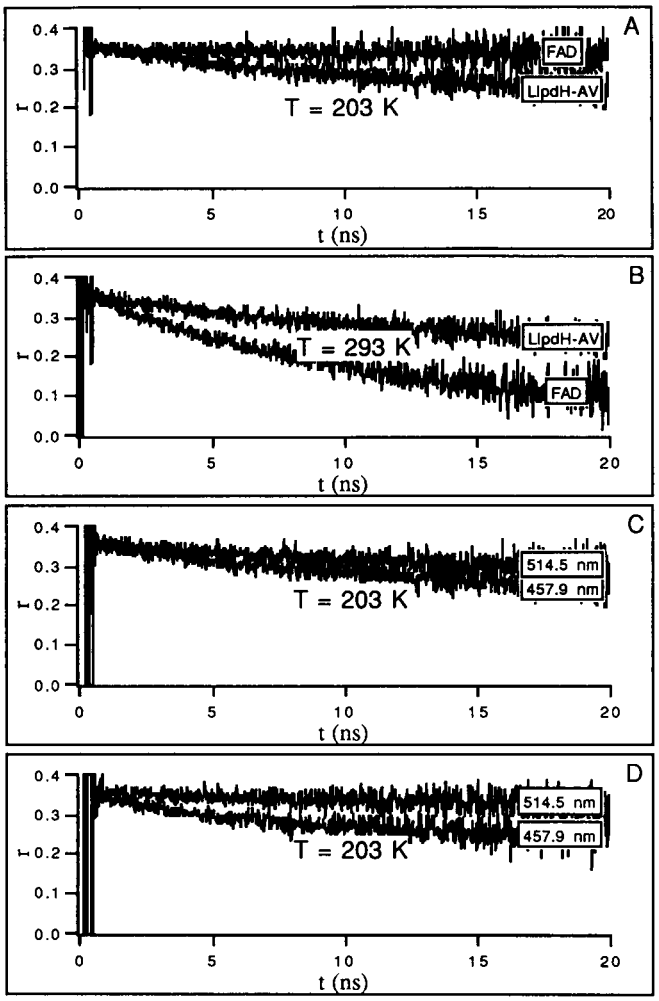

FIGURE 7 Temperature- and excitation wavelength-dependence of experimental time-dependent fluorescence anistropy. (*A* and *B*) Comparison of fluorescence anisotropy of free and protein-bound FAD at 203 and 293 K in 80% glycerol on main-band excitation (457.9 nm). (*C* and *D*) Fluorescence anisotropy of LipDH-AV (*C*) and LipDH-Δ14 (*D*) at 203 K in 80% glycerol on main-band (457.9 nm) and red-edge (514.5 nm) excitation.

Failure of energy transfer between like molecules is known to occur in systems where the dipolar relaxation time (τ_r) exceeds the average fluorescence lifetime (τ_f) (Demchenko, 1987; Nemkovich et al., 1991). Upon excitation of the proteins at 514.5 nm, we found an increase in the anisotropy as compared with the samples excited at 457.9 nm (Fig. 7, *C* and *D*). We thus have a second indication that the depolarization of the fluorescence is caused by energy transfer between the flavins. The magnitude of this effect and the relaxation rate of the anisotropy is dependent on the properties of the dipolar surroundings of the chromophores as outlined below.

The inverse Laplace transform of the fluorescence anisotropy decays (Fig. 8 *A*) on main-band excitation (457.9 nm) contains two regions of interest. At all mea-

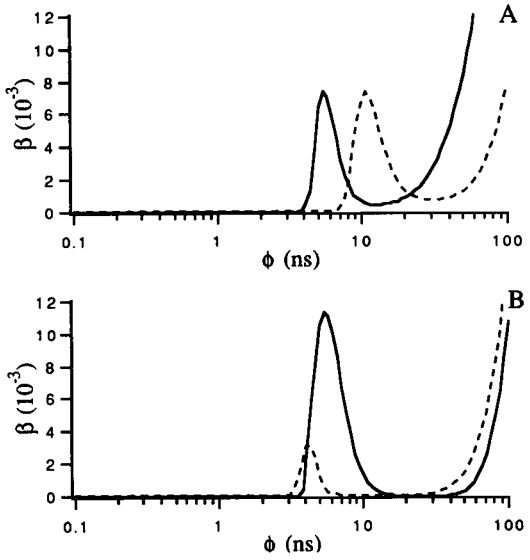

FIGURE 8 One-dimensional MEM analysis of fluorescence anisotropy decays of LipDH-AV (*A*) and LipDH-Δ14 (*B*) at 203 K. (——) Correlation-time spectrum obtained after 457.9 nm excitation. (- - -) Correlation-time spectrum obtained after 514.5 nm excitation.

sured temperatures (203–303 K), a peak is resolved for LipDH-AV with an integrated amplitude (scattered) around 0.08 ± 0.01. The barycenter (7.7 ± 1.5 ns) of this peak does not show a significant trend with temperature. At the long-correlation time edge of the spectrum, the amplitude continuously increases (Fig. 8 *A*). This limiting anisotropy of 0.28 ± 0.01 originates from the rotational immobilization of the protein in the highly viscous solvent on a time scale of fluorescence emission. The anisotropy decay is thus composed of a single relaxation process (or unimodel relaxation distribution) with a constant term. A similar correlation-time spectrum was found for LipDH-Δ14 with a somewhat shorter value for the average of the barycenters (5.1 ± 1.2 ns) and similar average sum of amplitudes (0.07 ± 0.02), taken over the measured temperature domain (Fig. 8 *B*).

Upon red-edge excitation (514.5 nm), the correlation-time spectrum is again composed of a unimodal distribution and a limiting anisotropy in both proteins (Fig. 8, *A* and *B*). However, the integrated amplitude of the unimodal distribution around 5 ns in LipDH-Δ14 is strongly diminished upon red-edge excitation at 203 K (Fig. 8 *B*) and only a slight decrease of total amplitude is observed for LipDH-AV.

To quantify these phenomena, let us assume that intersubunit energy transfer between the flavins is the physical mechanism that causes the observed depolarization of the fluorescence in lipoamide dehydrogenase. For a homogeneous binary system where the independent states have equal rates of depopulation of the excited state, the time-dependent anisotropy $r(t)$ is given by Tanaka and Mataga (1979):

$$r(t) = \frac{3}{5(r_1 + r_2)}\left[\frac{r_1k_{21} + r_2k_{12}}{k_{12} + k_{21}}(3\cos^2\delta - 1) + \frac{r_1k_{12} + r_2k_{21}}{k_{12} + k_{21}}(3\cos^2\theta - 1) + \left\{\frac{r_1k_{21} + r_2k_{12}}{k_{12} + k_{21}}(3\cos^2\delta - 1) - \frac{r_1k_{21} + r_2k_{12}}{k_{12} + k_{21}}(3\cos^2\theta - 1)\right\}e^{-(k_{12}+k_{21})t}\right] \quad (9)$$

where r_1 and r_2 are the fractional absorptions at excitation wavelength λ of monomer 1 and 2, respectively, and k_{12} and k_{21} are the rates of energy transfer from monomer 1 to 2 and vice versa. The parameters δ and θ in the preexponential amplitude and limiting anisotropy are the intramolecular and intermolecular angle, respectively, between absorption and emission transition moments in the binary system. The intermolecular angle of absorption and emission transition moments from monomer 1 to monomer 2 (θ_1) is equated to the intermolecular angle from monomer 2 to monomer 1 (θ_2), because these cannot be separately resolved (3 unknowns in a system of 2 linear equations). Note that in this expression the energy of transition from ground to excited state does not need to be the same in monomer 1 and 2. Upon main-band excitation of an inhomogeneously broadened system, the most probable energy configuration (Fig. 9 *A*) of monomer 1 and 2 is excited with equal probability, so that $r_1 = r_2$ and $k_{12} = k_{21} = k_T$. Equation 9 reduces to the expression derived by Tanaka and Mataga (1979) for a dimeric system with a unique spatial configuration:

$$r(t) = \frac{1}{10}[3\cos^2\delta + 3\cos^2\theta - 2 + \{3\cos^2\delta - 3\cos^2\theta\}e^{-2k_Tt}]. \quad (10)$$

The preexponential amplitude and the limiting anisotropy are functions of the relative geometrical arrangement of the transition moments of the interacting moieties. This geometrical arrangement is independent of temperature if there are no temperature-dependent conformational changes in the proteins. Consequently, when the data surface obtained from main-band excitation is fitted to an exponential anisotropy decay function plus a constant term,

$$r(t) = \beta_1 e^{(-t/\phi_T)} + \beta_2, \quad (11)$$

the amplitudes β_i must be physical invariants along the temperature axis.

Upon red-edge excitation, photoselection of nonequilibrium solvate energy configurations can take place even in a situation where the homogeneous bandwidth exceeds the inhomogeneous one (Nemkovich et al., 1991). A solvate is in this case defined as a fluorophore

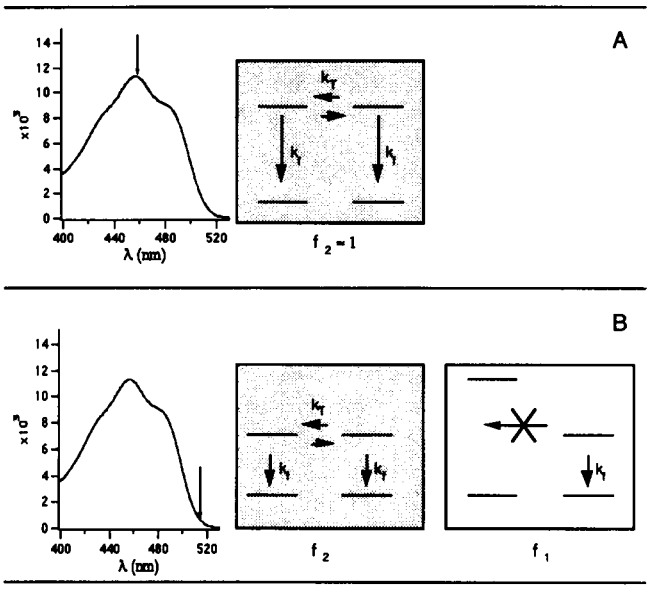

FIGURE 9 Compartmental model for excitation energy dependence of energy transfer. Absorption spectrum with an arrow on the excitation wavelength is shown together with a schematic energy diagram with ground and excited states in a dimer. k_T is the rate of energy transfer, k_f is the rate of fluorescence emission, f_1 is the fractional population of dimers in which energy transfer does not take place, and f_2 is the fractional population of dimers in which energy transfer occurs. (*A*) Main-band excitation. The fractional population of dimers in unfavorable energy configuration for transfer is approximately zero ($f_1 \approx 0$). (*B*) Red-edge excitation. A considerable fraction of excited dimers is in an energy configuration unfavorable for transfer ($f_1 > 0$). Note that the energy separations between ground and excited states in the red-edge excited molecules are smaller than in the case of main-band excitation.

and its immediate (protein) environment. In a system, with rapidly reorienting dipolar environment ($\tau_r \ll \tau_f$) in the high temperature regime, up-relaxation causes emission or weak dipole-dipole interaction to take place from a nonequilibrium energy state, irrespective of excitation wavelength. Consequently, the system is analogous to the main-band excited case and the β_i should be physical invariants of excitation wavelength and temperature. When dipolar relaxation is much slower than fluorescence emission ($\tau_r \gg \tau_f$), up-relaxation is slowed down and energy transfer or emission of a photon will take place from a nonequilibrium excited state with minimal energy separation between ground and excited state (Demchenko, 1987; Nemkovich et al., 1991). In this case the most probable energy configuration of the dimer will be that of a nonequilibrium excited state together with an acceptor in an equilibrium ground state energy configuration (Fig. 9 *B*). In this configuration, energy transfer will be endothermic and cannot take place. It will only take place in dimers where the acceptor-protein matrix system has equal or smaller magnitude of the transition energy than the excited donor. The system can be treated as consisting of two compartments. One compartment with a fractional population of f_1 that is not able to transfer energy and one compartment with fractional population of f_2 that is able to transfer energy ($f_1 + f_2 = 1$). The expression for the anisotropy decay is constructed from Weber's addition law (Weber, 1952), assuming that both compartments have equal quantum yields:

$$r(t) = \frac{1}{10}[3(2 - f_2)\cos^2\delta + 3f_2\cos^2\theta - 2 + f_2\{3\cos^2\delta - 3\cos^2\theta\}e^{-2k_T t}]. \quad (12)$$

The anisotropy is again described by an exponential and constant term analogous to Eq. 11. In case of red-edge excitation, the β_i are not physical invariants of temperature because f_2 is dependent on the dipolar relaxational properties of the protein matrix and on photoselection of nonequilibrium solvates. From the anisotropy decay curves obtained after main-band excitation, the δ and θ can be determined so that the fractional populations (f_1, f_2) can be calculated from the amplitudes of the red-edge excited anisotropy decays.

The additional relation we can impose upon the parameters of Eq. 11 at different temperatures (T) and excitation wavelengths (λ) is between the correlation times of transfer $\phi_T(T, \lambda)$, which is reciprocally related to the rate of energy transfer k_T:

$$\phi_T = \frac{1}{2k_T}. \quad (13)$$

The rate of energy transfer k_T is related to geometrical and spectral parameters by the Förster equation (Förster, 1948). The overlap integral J, which is a spectral parameter of the Förster equation, depends on the shape and relative position of the absorption and fluorescence emission spectrum of the interacting luminophores of the binary homotransfer system in question. J will be dependent on excitation wavelength and temperature since the emission spectrum is dependent on the dipolar relaxational properties of the protein matrix (Fig. 10 *A*). The $\phi_T(T_i, \lambda_j)$ are then related through the experimentally determined overlap integrals $J(T_i, \lambda_j)$:

$$\frac{\phi_T(T_i, \lambda_j)}{\phi_T(T_k, \lambda_l)} = \frac{J(T_k, \lambda_l)}{J(T_i, \lambda_j)}. \quad (14)$$

The abovementioned relations between parameters of the energy transfer model (Eq. 11) can be introduced as a priori knowledge into a global analysis of the anisotropy decay surfaces. The parameter link schemes can be represented in matrix notation where one dimension represents the parameters of the model and the other dimension the experiment number (Beechem and Gratton, 1988). Globally linked parameters will have the same logic number in the matrix. The large amount of experiments performed on the proteins made it impractical to list each experiment number separately in the global link matrix. Instead the experiments have been divided in two categories in Table 2. The division be-

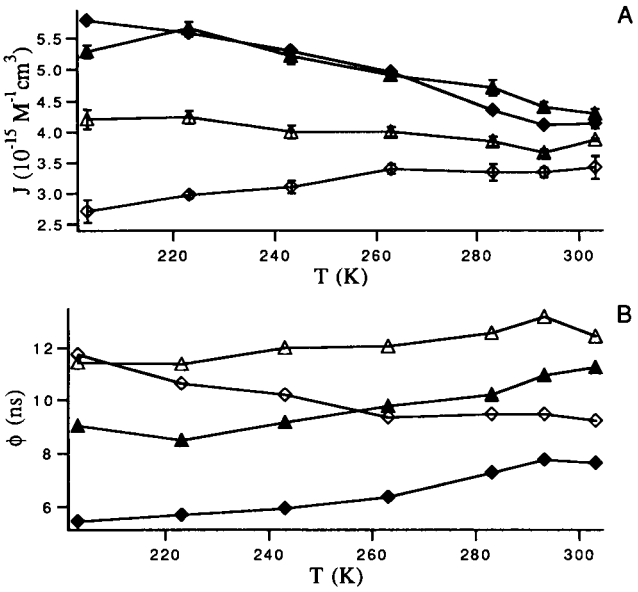

FIGURE 10 Temperature and excitation wavelength dependence of overlap integrals. (*A*) and transfer correlation-times (*B*). (▲) Data for LipDH-AV, (♦) Data for LipDH-Δ14, (△, ◇) Red-edge excitation (514.5 nm), (▲, ♦) Main-band excitation (457.9 nm).

tween categories is based on excitation energy. Two entries are presented in the matrix where the first numerical entry represents the intercategory linkage and the second alphabetical entry represents the intracategory linkage. The *J*-normalized transfer correlation time and amplitudes obtained from the global fit of the anisotropy data surfaces to Eq. 11 with the link scheme as in Table 2 are presented in Table 3, together with the global χ^2 when no linkages were imposed between the parameters. The values of the global χ^2 are close to unity and comparable in the two cases, indicating the correct implementation of the more stringent link scheme in Table 2. The residual surfaces were randomly scattered around a $z = 0$ surface (Fig. 11), which shows that Eq. 11 is a proper model to describe the anisotropy decay of LipDH-AV and LipDH-Δ14 in 80% glycerol.

By summation and subtraction of the amplitudes β_1 and β_2, information on intra- and intermolecular angles of absorption and emission transition moments in the isoalloxazines of the FADs in lipoamide dehydrogenase can be obtained:

$$\beta_2 + \beta_1 = {}^3/_5 \cos^2 \delta - {}^1/_5 \quad (15)$$

$$\beta_2 - \beta_1 = {}^3/_5 \langle \cos^2 \theta \rangle - {}^1/_5, \quad (16)$$

where the brackets in Eq. 16 denote an average of the two values ($\langle \cos^2 \theta \rangle = {}^1/_2[\cos^2 \theta_1 + \cos^2 \theta_2]$). In the isoalloxazine ring, the emission and absorption transition moments are not parallel, which manifests itself experimentally in a value of the anisotropy of 0.35 at time $t = 0$, which is lower than the fundamental anisotropy of 0.4. From Eq. 15, we obtained a value of 17° for δ. The direction of the absorption transition moment relative to the pseudo symmetry axis of the isoalloxazine ring is known ($\psi = -32°$) (Johansson et al., 1979), which gives two possibilities for the direction of the emission transition moment ($\zeta = -15°$ or $-49°$), provided that it lies in the plane of the molecule. The crystallographic coordinates of the isoalloxazine rings in LipDH-AV, together with the values of the anisotropy decay parameters β_1 and β_2, allow us to calculate the absolute position of the emission transition moment in the isoalloxazine ring bound to the dimeric protein. The angles θ_1 and θ_2 can be calculated from crystallographic coordinates and the directions of the absorption and emission transition moments in the molecular planes of both isoalloxazines in the subunits. For the direction of the emission transition moment, there are two possibilities, giving two sets of angles θ_1 and θ_2. From the direction of $\zeta = -47°$, we obtained a value of 0.37 for $\beta_2 - \beta_1$, which is in disagreement with the experimentally obtained value (0.14 for LipDH-AV; Table 3), whereas the direction $\zeta = -15°$ yielded $\beta_2 - \beta_1 = 0.13$ in closer agreement with experiment. With the directions of the transition moments known in the isoalloxazine ring, we can calculate the orientation factor κ^2 (Dale et al., 1979) from crystallographic data. We obtained the values $\kappa^2 = 3.23$ and $\kappa^2 = 3.35$ for both directions of energy transfer. An estimation of the distance between the centers of the isoalloxazines can be made by substituting the rate of transfer k_T and the experimental overlap integral $J(T, \lambda)$ in the Förster equation with a value for the refractive index $n = 1.4$ (Steinberg, 1971) and radiative rate $\lambda_d = 0.056$ ns^{-1} (Visser and Müller, 1979). The calculated distances can be compared with the distance directly obtained from crystallographic coordinates in LipDH-AV. In case that the orientation factor would be an unknown, only an upper limit of the distance can be calculated (Dale et al., 1979). The interflavin distance and angular parameter θ derived from fluorometric and crystallographic data are in excellent agreement for LipDH-AV (Table 4), which shows the validity of the model used. In comparison, the upper limit for the distance between the prosthetic groups is slightly smaller and the angle θ is slightly larger for LipDH-Δ14. This result suggests that the geometric ar-

TABLE 2 Link matrix*

Type of experiment	Parameters		
	β_1	β_2	ϕ_T‡
λ_{ex} = 457.9 nm	1	3	5
80% glycerol T = 203–303 K	AL	AL	AL
λ_{ex} = 514.5 nm	2	4	5
80% glycerol T = 203–303 K	NL	NL	AL

* AL, all parameters within category linked. NL, all parameters within category not linked.
‡ Transfer correlation time linked by a $1/J(T, \lambda_{ex})$ vector.

TABLE 3 **Fluorescence anisotropy fit parameters**

Sample	β_1	β_2	ϕ_T (ns)	Global χ^2 Linked	Global χ^2 Unlinked
LipDH-AV	0.106*	0.245*	8.46*	1.01	1.00
	(0.098–0.120)	(0.228–0.252)	(6.8–11.2)		
	0.0759‡	0.279‡	7.73‡		
	(0.014)	(0.015)	(1.52)		
LipDH-Δ14	0.0909*	0.260*	5.43*	1.04	1.02
	(0.090–0.102)	(0.248–0.263)	(4.5–7.2)		
	0.0675‡	0.283‡	5.12‡		
	(0.023)	(0.022)	(1.21)		

* Values as obtained from the global analysis of the data surface. The numbers in parentheses are the errors as determined from a rigorous error analysis with a 67% confidence interval.

‡ Average values as obtained from the MEM analysis of the individual decay curves. The average was taken from the inverse Laplace transforms of the decays at seven temperatures (203–303 K). The numbers in parentheses are the standard deviations.

rangement of the subunits in LipDH-Δ14 is different to that of the wild-type enzyme.

The transfer correlation time $\phi_T(T, \lambda)$ as function of temperature is shown in Fig. 10 *B*. Because of the red-shift of the emission spectra on 514.5 nm excitation with a concomitant decrease in J as compared with main-band excitation, an increase of the transfer correlation time is obtained upon red-edge excitation. The decrease of the probability of energy transfer upon edge excitation is not uniform for the wild-type and mutant proteins. The values of $\phi_T(T, 514.5)$ of LipDH-Δ14 exhibit a much stronger temperature dependence and converge to the values of $\phi_T(T, 457.9)$ on increase of temperature. The convergence of the $\phi_T(T, \lambda)$ in LipDH-Δ14 shows

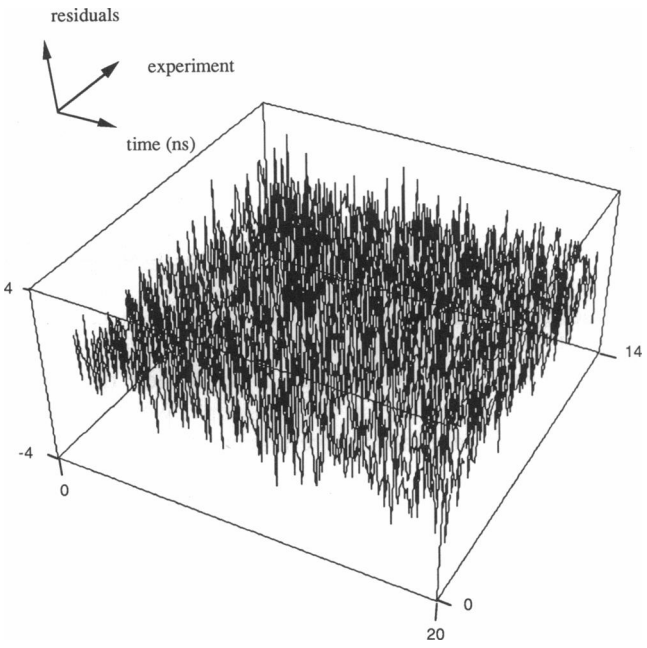

FIGURE 11 Weighted fluorescence anisotropy decay residual surface of the global fit of the fluorescence anisotropy decay of LipDH-AV to Eqs. 10 and 12.

that the dipolar surroundings of the isoalloxazines is converted from a solid-state environment ($\tau_r \gg \tau_f$) to an environment with efficient dipolar relaxation ($\tau_r \ll \tau_f$). The $\phi_T(T, \lambda)$ values of LipDH-AV do not converge as efficiently, indicating a highly rigid environment in the measured temperature domain.

The fractional population of transferring molecules (f_2) at a certain temperature can be calculated from the ratio of β_1 obtained at red-edge and main-band excitation (Fig. 12 *A* and *B*). Comparison of the f_2 values of the two proteins at 203 K shows that the fractional population of photoselected nonequilibrium solvates in LipDH-AV is much smaller than for LipDH-Δ14. The magnitude of the selection function depends on the relative width of the inhomogeneous broadening function as compared with the homogeneous broadening function. The deletion mutant has thus a more heterogeneous population of active sites as compared with the wild-type enzyme. Furthermore, the fractional population of transferring protein molecules increases with temperature in LipDH-Δ14, whereas f_2 is practically temperature invariant in LipDH-AV.

The increase of f_2 with temperature in the deletion mutant is caused by a transition from a static to a dynamic inhomogeneously broadened system. Rapid relaxation of the surrounding (solvent) dipoles at higher temperatures causes energy transfer to take place from equilibrium excited states. It is remarkable that f_2 does not reach unity, whereas rapid relaxation is observed for free FAD in 80% glycerol at temperatures above 263 K (Bastiaens et al., 1992*a*). This result is in agreement with a model where the modulation of the solvate energy levels is governed by two environments: one with a small activation energy (solvent relaxation) and one with a higher activation energy (protein relaxation).

DISCUSSION

In both LipDH-AV and LipDH-Δ14 in 80% glycerol, we observed a minimum of two lifetime classes as revealed

TABLE 4 **Geometric parameters**

Sample	Geometry from anisotropy decay parameters			Geometry from crystallographic data		
	R*	δ‡	θ§	R‖	θ_1¶	θ_2‡
	nm	°	°	*nm*	°	°
LipDH-AV	4.0 (3.8–4.2)	16.6 (16.6–17.1)	138.7 (135.8–140.2)	3.9	138.4	137.9
LipDH-Δ14	3.7 (3.6–3.9)	16.6 (16.3–16.8)	141.7 (139.4–142.0)	—	—	—

* Interflavin distance as obtained from the Förster equation with n = 1.4, λ_d = 0.0556 ns^{-1}, and κ^2 = 3.29.
‡ Intramolecular angle between absorption and emission moments obtained from Eq. 18.
§ Intermolecular angle between absorption and emission moments obtained from Eq. 19.
‖ Interflavin distance calculated from crystallographic coordinates where the center of the isoalloxazines has been taken in the middle of the N5 and N10 atoms.
¶ Intermolecular angle between absorption and emission from crystallographic coordinates in both directions of energy transfer.
Numbers in parentheses are the errors as determined from the rigorous error analysis with a 67% confidence interval.

by the inverse Laplace transforms of the fluorescence decays. Decrease of the fractional contribution of the shorter lifetime class on lowering the temperature establishes that the two lifetime classes correspond to conformational substates of the proteins. A relatively large (>50 kJ/mol) undetermined activation barrier exists between the states, since the interconversion was slow on a fluorescence time scale. The high activation energy of transition between the two states possibly classifies them as conformational substates of the first tier (CS^1) (Austin et al., 1975; Frauenfelder and Gratton, 1986; Frauenfelder et al., 1988). In contrast, the rate of exchange between conformational substates in LipDH-AV in aqueous solution is in the order of the fluorescence lifetime (Bastiaens et al., 1992*b*). The large effect of the solvent viscosity on the transition frequency indicates that considerable protein-domain rearrangements must be involved in the transition between the two conformers. An additional conformational state with higher transition enthalpy is also populated in aqueous solution. In 80% glycerol, protein dynamics is damped and the correlated atom movements do not contain enough kinetic energy to overcome the activation barrier to populate this conformational substate with higher enthalpy. The Gibbs free energy difference between conformational states is comparable in the wild-type and mutant protein. However, the van 't Hoff plot of the conformational equilibrium constant is not linear below 263 K in case of the mutant protein. Equilibrium is then not established below 263 K due to a larger activation barrier between conformational states in LipDH-Δ14 as compared with LipDH-AV. Removal of the 14 COOH-terminal amino acids by site-directed mutagenesis apparently affects the activation energy between the conformational states.

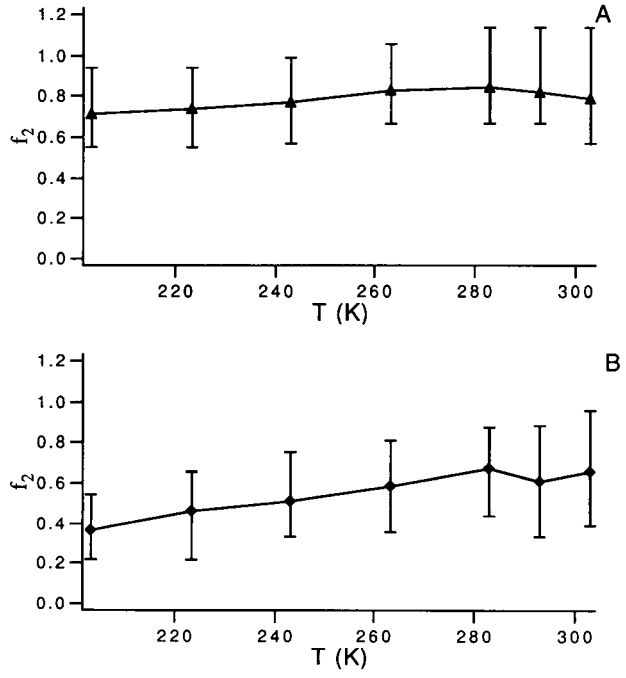

FIGURE 12 Fractional population (f_2) of transferring molecules on edge excitation. (*A*) Data for LipDH-AV. (*B*) Data for LipDH-Δ14.

Both the maximum entropy method and the global analysis of the results revealed that the temperature dependence of the two observed lifetime classes is well described by one thermally activated and one temperature-independent radiative constant. By iodide quenching and molecular relaxation spectroscopy, we have shown that the flavins are more solvent accessible in the mutant protein (Bastiaens et al., 1992*a*). The difference in the values of the rate constants and the effective activation energy of thermal quenching both reflect the difference in local environment of the flavins in the two proteins. The frequency factor and the effective activation energy of thermal quenching are smaller for the solvent accessible flavins in the mutant than for the flavins in the wild-type enzyme. In addition, the temperature-independent rate constants are larger for the flavins in LipDH-Δ14. It is then tempting to assign the smaller lifetime class of

LipDH-AV, with the lower activation energy, smaller frequency factor, and larger temperature-independent rate constant, to a more "open" (substrate accessible) protein conformation.

The decrease in width of the lifetime distributions with increase in temperature possibly reflects rapid transitions between conformational substates of the third tier (CS^3) (Frauenfelder and Gratton, 1986). From the slope of the FWHM on Arrhenius coordinates, the empirical activation energy associated with this process was found to be between 4 and 20 kJ/mol. The magnitude of this activation energy is comparable with that of thermal quenching and possibly reflects the same dynamic mechanism (transitions between CS^3). The local flavin environments in wild-type and mutant lipomide dehydrogenase have distinct dynamic and structural properties as revealed by a smaller number of CS^3 and lower activation barrier between states of tier 3 in LipDH-Δ14, in agreement with the conclusions drawn from the parameters of thermal quenching of the fluorescence.

From the global analysis of fluorescence anisotropy data surface obtained at different temperatures and excitation wavelengths, we could demonstrate that homoenergy transfer between the two flavins in both subunits of LipDH-AV is a mechanism that causes depolarization of the fluorescence. Red-edge spectroscopy in conjunction with temperature variation provides the necessary experimental axes to assess diagnostic methods to discriminate between reorientational dynamics and energy transfer. We can therefore exclude restricted motion of the flavins or hinge motion of the subunits as alternative mechanisms causing depolarization of the fluorescence (de Kok and Visser, 1987).

LipDH-AV is an example of a biological macromolecule that can be used to test the validity of models describing the effect of excitation energy and dipolar relaxation on energy transfer between like chromophores. The capability of model testing arises from (*a*) the known crystal structure, (*b*) the unique orientation of the nonmobile flavins, and (*c*) the possibility to alter the electronic properties of the active site by site-directed mutagenesis. The physical relations between the parameters of an anticipated model describing the anisotropy decay at different experimental conditions can be exploited by the use of global fit procedures in the analysis of data surfaces. The compartmental model used to describe the anisotropy decay surfaces of the proteins is a discrete state approximation of a qualitative physical model on failure of energy transfer (Demchenko, 1987; Nemkovich et al., 1991). In a static inhomogeneously broadened system ($\tau_r \gg \tau_f$), the pure electronic transition energies are distributed as some continuous function (e.g., Gaussian). The experimental overlap integral J_{exp} of a dimeric system is then a static average of the overlap integrals J_i of the populations of dimers in energy configuration i:

$$J_{exp} = \sum_{i=1}^{n} A_i J_i \qquad (17)$$

where A_i is the fractional population of dimers in energy configuration i. The rate of intersubunit energy transfer is then also a distributed function. In our model we assume that there is a predominant population (A_j) of dimers with energy configuration j within the population f_2. This energy configuration j corresponds to equal transition energies of donor and acceptors. J_{exp} is then an overestimation of J_j, and the rate of transfer k_T is a weighted average of the rates of each population i. In a dynamic inhomogeneously broadened system ($\tau_r \ll \tau_f$), all energy configurations are sampled during energy transfer and J_{exp} and thus k_T are dynamic averages (Dale et al., 1979). The system behaves as if a single energy configuration j is present in all dimers. The rate of transfer k_T has then a discrete value independent of excitation energy proportional to J_{exp}. The model of Tanaka and Mataga (1979) (Eq. 10) is then adequate. Despite these assumptions in our model, we obtained good agreement with experimental data. From the amplitudes of the anisotropy decay and transfer correlation time, geometrical information concerning the relative orientation and distance of the isoalloxazinic residues of the flavins in the subunits is obtained. The results as obtained for LipDH-AV are in excellent agreement with crystallographic data that validates the energy transfer model used. The interflavin distance and angle are slightly different in LipDH-Δ14 that is possibly caused by the perturbed interaction between the subunits.

The transfer correlation times and the fractional population of transferring molecules (f_2) are approximately temperature independent for LipDH-AV that we attribute to a rigid dipolar environment ($\tau_r \gg \tau_f$) of the flavins in the temperature range studied. The large population of transferring molecules (f_2) and the relatively small increase of the transfer correlation time on edge excitation at 203 K shows that the photoselection of nonequilibrium solvates is small on excitation at 514.5 nm. The inhomogeneous bandwidth is thus small and the isoalloxazines are located in a highly homogeneous, rigid (dipolar) protein environment. The temperature dependence of $\phi_T(T, 514.5)$ and f_2 in LipDH-Δ14 shows that effective dipolar relaxation takes place in this protein on increase of the temperature. The interaction of the solvent dipoles with the isoalloxazines causes an increased inhomogeneity of the surrounding dipolar structure. At low temperatures (203 K) the immobilized solvent dipoles increase the inhomogeneous bandwidth as compared with the situation in the wild-type enzyme. The increased inhomogeneous bandwidth results in an enhanced photoselection of nonequilibrium solvates and larger shift of the emission spectra on edge excitation. These factors contribute to red-edge failure of energy transfer by decreasing the overlap integral and the popu-

lation of transferring molecules (f_2). Above 240 K, the fluctuating solvent dipoles cause partial up-relaxation and a decrease in the transfer correlation time at edge excitation. The more structured protein matrix surrounding the flavins hinders complete up-relaxation, and failure of energy transfer is still observed at high temperature, although to a lesser extent.

The reduced lipoamide [Lip(SH_2)]/oxidized form of nicotinamide adenine dinucleotide activity of LipDH-Δ14 in the dimeric form is extremely low (<0.1% of wild-type activity), whereas the diaphorase (reduced form of nicotinamide adenine dinucleotide/dichlorophenyl-idophenol) activity is ~50% of the wild-type enzyme. Although the dissociation constant of the subunits is three orders of magnitude larger (Schulze et al., 1991), the mutated protein is present as a dimer under our experimental conditions. The removal of the 14 COOH-terminal amino acids has thus a most drastic effect on the Lip(SH_2) binding site that comprises amino acid residues from both subunits (Mattevi et al., 1991). Since the Lip(SH_2) binding site is composed of amino acid residues of both subunits and removal of the 14 COOH-terminal amino acids destabilizes the dimer, it is tempting to postulate that the COOH-terminal polypeptide of one subunit in LipDH-AV interacts via the Lip(SH_2) binding site of the other subunit and thereby stabilizes the dimer. The results as obtained in this study clearly demonstrate that the "disordered" COOH-terminal polypeptide in LipDH-AV has an important effect on the local isoalloxazine microenvironment in LipDH-AV. We expect that the COOH-terminal tail folds back into the Lip(SH_2) binding site, thereby shielding the active site from the solvent. One question remains open: what is the catalytic function of the two major conformations observed in the wild-type enzyme in aqueous solution? If they do correspond to an "open" [(Lip(SH_2) can bind] and "closed" [Lip(SH_2) cannot bind] enzyme conformation, the rate-limiting step in catalysis could be the establishment of equilibrium between the two states in case the activation barrier between them is sufficiently large. To test this hypothesis substrate analogue, binding studies must be undertaken. It is then expected that binding will result in the collapse of the enzyme into a single conformation.

We thank Dr. C. Veeger for valuable discussions.

This research was supported in part by the Netherlands Organization for Scientific Research (NWO).

Received for publication and in final form 3 March 1992.

REFERENCES

Alcala, R. J., E. Gratton, and F. G. Prendergast. 1987. Fluorescence lifetime distributions in proteins. *Biophys. J.* 51:597–604.

Austin, R. H., K. W. Beeson, L. Eisenstein, H. Frauenfelder, and I. C. Gunsalus. 1975. Dynamics of ligand binding to myoglobin. *Biochemistry.* 14:5355–5373.

Bastiaens, P. I. H., P. J. M. Bonants, F. Müller, and A. J. W. G. Visser. 1989. Time-resolved fluorescence spectroscopy of NADPH-cytochrome P-450 reductase: demonstration of energy transfer between the two prosthetic groups. *Biochemistry.* 28:8416–8425.

Bastiaens, P. I. H., A. van Hoek, W. J. H. van Berkel, A. de Kok, and A. J. W. G. Visser. 1992*a*. Molecular relaxation spectroscopy of flavin adenine dinucleotide in wild type and mutant lipoamide dehydrogenase from *Azotobacter vinelandii. Biochemistry.* In press.

Bastiaens, P. I. H., A. van Hoek, W. F. Wolkers, J. C. Brochon, and A. J. W. G. Visser. 1992*b*. Comparison of the dynamical structures of lipoamide dehydrogenase and glutathione reductase by time-resolved polarized flavin fluorescence. *Biochemistry.* In press.

Beechem, J. M., and E. Gratton. 1988. Fluorescence spectroscopy data analysis environment: a second generation global analysis program. *Proc. SPIE.* (The International Society for Optical Engineering) 909:70–81.

Beechem, J. M., E. Gratton, M. Ameloot, J. R. Knutson, and L. Brand. 1991. The global analysis of fluorescence intensity and anisotropy decay data. *In* Topics in Fluorescence Spectroscopy. Vol. 2. J. R. Lakowicz, editor. Plenum Press, New York. 241–305.

Dale, R. E., J. Eisinger, and W. E. Blumberg. 1979. The orientational freedom of molecular probes. The orientation factor in intramolecular energy transfer. *Biophys. J.* 26:161–194.

de Kok, A., and A. J. W. G. Visser. 1984. Mobility of lipoamide dehydrogenase in and out of the pyruvate dehydrogenase complex from *Azotobacter vinelandii. In* Flavins and Flavoproteins. R. C. Bray, P. C. Engel, and S. G. Mayhew, editors. Walter de Gruyter, Berlin. 149–152.

de Kok, A., and A. J. W. G. Visser. 1987. Flavin binding site differences between lipoamide dehydrogenase and glutathione reductase as revealed by static and time-resolved flavin fluorescence. *FEBS (Fed. Eur. Biochem. Soc.) Lett.* 218:135–138.

de Kok, A., H. J. Bosma, A. H. Westphal, and C. Veeger. 1988. A comparison between the subunit organization of the pyruvate dehydrogenase complexes from *Azotobacter vinelandii* and *Escherichia coli.* Does a unifying model exist for the complexes from gram-negative bacteria? *In* Thiamine Pyrophosphate Biochemistry. Vol. 2. R. Schowen and A. Schellenberger, editors. CRC Press, Boca Raton, FL. 19–36.

Demchenko, A. P. 1987. Ultraviolet Spectroscopy of Proteins. Springer-Verlag, Berlin.

Förster, Th. 1948. Zwischenmolekulare energiewanderung und fluoreszenz. *Ann. Physik.* 2:55–75.

Frauenfelder, H. and E. Gratton. 1986. Protein dynamics and hydration. *Methods Enzymol.* 127:207–216.

Frauenfelder, H., F. Parak, and R. D. Young. 1988. Conformational substates in proteins. *Annu. Rev. Biophys. Biophys. Chem.* 17:451–479.

Galley, J. A., and G. M. Edelman. 1962. The effect of temperature on the fluorescence of some aromatic amino acids and proteins. *Biochim. Biophys. Acta.* 60:499–509.

Gentin, M., M. Vincent, J. C. Brochon, A. K. Livesey, N. Cittanova, and J. Gallay. 1990. Time-resolved fluorescence of the single tryptophan residue in rat α-fetoprotein and rat serum albumin: analysis by the maximum-entropy method. *Biochemistry.* 29:10405–10412.

Gratton, E., D. M. Jameson, and R. D. Hall. 1984. Multifrequency phase and modulation fluorometry. *Annu. Rev. Biophys. Bioeng.* 13:105–124.

Johansson, L. B.-Å., Å., Davidsson, G. Lindblom, and K. Razi Naqvi. 1979. Electronic transitions in the isoalloxazine ring and orientation of flavins in model membranes studied by polarized light spectroscopy. *Biochemistry.* 18:4249–4253.

Lakowicz, J. R., G. Laczko, and I. Gryczynski. 1986. 2-GHz frequency-domain fluorometer. *Rev. Sci. Instrum.* 57:2499–2506.

Livesey, A. K., and J. C. Brochon. 1987. Analyzing the distribution of decay constants in pulse-fluorimetry using the maximum entropy method. *Biophys. J.* 52:693–706.

Mattevi, A., A. J. Schierbeek, and W. G. J. Hol. 1991. Refined crystal structure of lipoamide dehydrogenase from *Azotobacter vinelandii* at 2.2 Å resolution. A comparison with the structure of glutathione reductase. *J. Mol. Biol.* 220:975–994.

Mérola, F., R. Rigler, A. Holmgren, and J. C. Brochon. 1989. Picosecond tryptophan fluorescence of thioredoxin: evidence for discrete species in slow exchange. *Biochemistry.* 28:3383–3398.

Nemkovich, N. A., A. N. Rubinov, and V. I. Tomin. 1991. Inhomogeneous broadening of electronic spectra of dye molecules. *In* Topics in Fluorescence Spectroscopy. Vol. 2. J. R. Lakowicz, editor. Plenum Press, New York. 367–428.

O'Connor, D. V., and D. Phillips. 1984. Time-Correlated Single Photon Counting. Academic Press, London.

Reed, L. J. 1974. Multi-enzyme complexes. *Acc. Chem. Res.* 7:40–46.

Rubinov, A. N., and V. I. Tomin. 1970. Bathochromic luminescence in low-temperature solutions of dyes. *Optics Spectrosc. (USSR),* 29:1082–1086.

Schulze, E., J. A. E. Benen, A. H. Westphal, and A. de Kok. 1991. Interaction of lipoamide dehydrogenase with the dihydrolipoyl transacetylase component of the pyruvate dehydrogenase complex from *Azotobacter vinelandii. Eur. J. Biochem.* 200:29–34.

Spencer, R. D., and G. Weber. 1972. Thermodynamic and kinetics of the intramolecular complex in flavin-adenine dinucleotide. *In* Structure and Function of Oxidation and Reduction Enzymes. Å. Åkeson, and A. Ehrenberg, editors. Pergamon Press, Oxford. 393–399.

Steinberg, I. Z. 1971. Long-range nonradiative transfer of electronic excitation energy in proteins and polypeptides. *Annu. Rev. Biochem.* 40:83–114.

Tanaka, F., and N. Mataga. 1979. Theory of time-dependent photo-selection in interacting fixed systems. *Photochem. Photobiol.* 29:1091–1097.

van Hoek, A., and A. J. W. G. Visser. 1981. Pulse selection system with electro-optic modulators applied to mode-locked CW lasers and time-resolved single photon counting. *Rev. Sci. Instrum.* 52:1199–1205.

van Hoek, A., and A. J. W. G. Visser. 1985. Artefact and distortion sources in time-correlated single photon counting. *Anal. Instrum.* 14:359–378.

van Hoek, A., K. Vos, and A. J. W. G. Visser. 1987. Ultrasensitive time-resolved polarized fluorescence spectroscopy as a tool in biology and medicine. IEEE (Inst. Electr. Electron. Eng.) *J. Quantum Electron.* 23:1812–1820.

Visser, A. J. W. G. 1984. Kinetics of stacking interactions in flavin adenine dinucleotide from time-resolved flavin fluorescence. *Photochem. Photobiol.* 40:703–706.

Visser, A. J. W. G. 1989. Time-resolved fluorescence studies of flavins. *In* Fluorescent Biomolecules. D. M. Jameson, and G. D. Reinhart, editors. Plenum Publishing Corp., New York. 319–341.

Visser, A. J. W. G., and F. Müller. 1979. Absorption and fluorescence studies on neutral and cationic isoalloxazines. *Helv. Chim. Acta.* 62:593–608.

Visser, A. J. W. G., H. J. Grande, F. Müller, and C. Veeger. 1974. Intrinsic luminescence studies on the apoenzyme and holoenzyme of lipoamide dehydrogenase. *Eur. J. Biochem.* 45:99–107.

Visser, A. J. W. G., H. J. Grande, and C. Veeger. 1980. Rapid relaxation processes in pig heart lipoamide dehydrogenase revealed by subnanosecond resolved fluorometry. *Biophys. Chem.* 12:35–49.

Visser, A. J. W. G., N. H. G. Penners, W. J. H. van Berkel, and F. Müller. 1984. Rapid relaxation processes in p-hydroxybenzoate hydroxylase from *Pseudomonas fluorescens* revealed by subnanosecond-resolved laser-induced fluorescence. *Eur. J. Biochem.* 143: 189–197.

Vos, K., A. van Hoek, and A. J. W. G. Visser. 1987. Application of a reference convolution method to tryptophan fluorescence in proteins. A refined description of rotational dynamics. *Eur. J. Biochem.* 165:55–63.

Wahl, P., J. C. Auchet, A. J. W. G. Visser, and C. Veeger. 1975. A pulse fluorometry study of lipoamide dehydrogenase. *Eur. J. Biochem.* 50:413–418.

Weber, G. 1952. Polarization of the fluorescence of macromolecules. Theory and experimental method. *Biochem. J.* 51:145–155.

Westphal, A. H., and A. de Kok. 1988. Lipoamide dehydrogenase from *Azotobacter vinelandii.* Molecular cloning, organization and sequence analysis of the gene. *Eur. J. Biochem.* 172:299–305.

Williams, C. H., Jr. 1976. Flavin containing dehydrogenases. Vol. 13. *In* The Enzymes. P. D. Boyer, editor. Academic Press, New York. 89–173.